Chapter 5
Nested Surface Coils for Multinuclear NMR

Arthur W. Magill and Rolf Gruetter

Laboratory of Functional and Metabolic Imaging, Ecole Polytechnique Federale de Lausanne, CH-1015 Lausanne, Switzerland
Department of Radiology, University of Lausanne, CH-1015 Lausanne, Switzerland
Department of Radiology, University of Geneva, CH-1211 Geneva, Switzerland

5.1 INTRODUCTION

A surface coil is any radiofrequency (RF) coil placed directly on the surface of the subject. Surface coils represent some of the simplest coil designs used in magnetic resonance, but are commonly used in experiments requiring the highest possible sensitivity.

In contrast to volume coils, which are designed to provide homogeneous sensitivity over the whole field-of-view, surface coils sacrifice field homogeneity to maximize the signal-to-noise ratio (SNR) over a limited region. Figure 5.1 shows an image of a mouse head, acquired with a volume and a surface coil. The volume coil gives a uniform image of the whole head—note that the brain occupies a relatively small part of that volume. While the NMR signal can be localized using field gradients, thermal noise cannot; coils are therefore sensitive to noise generated over their entire field-of-view. By designing a coil with a reduced field-of-view, for example covering only the brain, the noise level is immediately reduced without affecting the signal level. This is the principle by which a surface coil increases the SNR.

The image shown in Figure 5.1(b) is typical for a surface coil. It is bright close to the coil, but the intensity falls off rapidly with increasing depth into the sample. This is the main difficulty when using a surface coil—the RF transmit power that produces a 180° nutation at one location in the sample will give a much larger nutation closer to the coil and a lower nutation further from it, making it difficult to, for example, produce a spin echo. To overcome this problem, adiabatic RF pulses are routinely used with surface coils, which, above a certain B_1 threshold, produce the same nutation independent of B_1 amplitude.[1]

Surface coils are usually designed for a specific application, restricting the field-of-view to cover only the anatomy of interest (a particular brain region, liver, heart, etc.) to minimize the noise sensitivity. Surface coils can be used in receive-only mode, in combination with a suitable volume transmit coil, or as transmit-receive coils; the latter being more common in multinuclear applications.

Surface coils are regularly used for proton studies, but their main application is for non-proton

RF Coils for MRI
Edited by J. Thomas Vaughan and John R. Griffiths

 ISBN: 978-0-470-77076-4

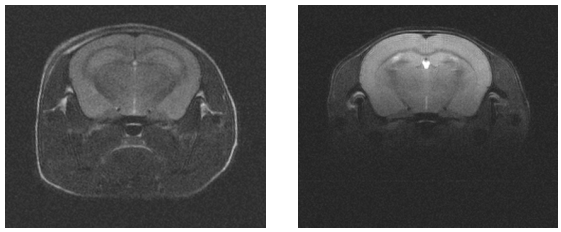

Figure 5.1. Images of a mouse brain, acquired with (a) a volume coil and (b) a surface coil.

acquisitions, especially spectroscopy, where it is often not possible to achieve the required SNR with a volume coil. Indeed, the first reported use of a surface coil was to study ^{31}P, where the increased SNR allowed phosphorus to be investigated in vivo for the first time.[2]

5.2 MULTINUCLEAR MRI AND MRS

The vast majority of in vivo magnetic resonance experiments are performed using protons (^{1}H). Protons have a high gyromagnetic ratio (giving high NMR sensitivity), and are present in large quantities in the body, mostly in the form of water. However, other nuclei can be studied in vivo, potentially giving access to information not available from proton imaging or spectroscopy.

After protons, the most commonly investigated nuclei are phosphorus (^{31}P), carbon (^{13}C), and sodium (^{23}Na).[3] A comparison of the NMR properties of these nuclei is given in Table 5.1. Phosphorus magnetic resonance spectroscopy (MRS) is used to investigate tissue energy metabolism. Phosphorous-31 has a relatively large gyromagnetic ratio, and 100% natural abundance, so produces a reasonably large NMR signal. Carbon-13 is a more challenging nucleus, as it has a lower natural abundance (1.1%) and a lower gyromagnetic ratio. However, it can be used to investigate almost every metabolic pathway in the body. While phosphorus and carbon are commonly investigated via spectroscopy, sodium (^{23}Na) is usually imaged. Sodium-23 has 100% natural abundance, but is present in relatively low concentration in the body; however, its distribution is very inhomogeneous. Sodium is used to investigate tissue damage, such as that caused by stroke or cancer.

Table 5.1. Properties of some biologically interesting NMR active nuclei[3]

Nucleus	Spin	Gyromagnetic ratio MHz/T	γ_X/γ_{1H}	Relative sensitivity
^{1}H	1/2	42.58	1.00	100
^{13}C	1/2	10.71	0.25	1.6
^{23}Na	3/2	11.27	0.26	1.8
^{31}P	1/2	17.25	0.41	6.9

It is often useful to "double tune" a non-proton probe, enabling it to excite and detect an NMR signal at two (or more) frequencies—commonly that of the nucleus we wish to investigate and of proton. There are several reasons for wanting to add a proton channel to a non-proton coil. First, as the proton signal is always stronger than that from other nuclei, a proton channel is useful for quickly acquiring a scout image. The scout can then be used to plan the non-proton acquisition, based on the actual anatomy of the animal or volunteer. A proton channel is also useful for shimming the main field. A well-shimmed B_0 field is critical when attempting to detect a weak NMR signal, but it is difficult to set up the shim using a weak signal. As the shim is independent of the nucleus, adding a proton channel allows the magnet to be shimmed using the stronger proton signal, before switching to the non-proton channel (without moving the sample) to perform the actual experiment.

A second RF field, at the proton frequency, may also be used to enhance the signal on the X-channel, via nuclear Overhauser effect (NOE), polarization transfer, and/or J-decoupling (usually simply called *decoupling*, causing much confusion for the coil designer!). In heteronuclear spin systems, such as ^{13}C–^{1}H, the polarization of the observed nuclei can be significantly enhanced by saturating the higher γ nuclei, giving rise to the NOE.[1] The maximum enhancement available due to NOE for a particular pair of spin systems is $1 + \gamma_I/(2\gamma_S)$, where γ_I and γ_S are the respective gyromagnetic ratios. For ^{13}C–^{1}H, for example, the potential enhancement is almost a factor of three. Alternatively, polarization of the observed nuclei can be enhanced via J-coupling methods, such as INEPT, which transfer polarization from the coupled to the observed nuclei by simultaneously exciting both.[1] In this case, the maximum enhancement factor is γ_I/γ_S, giving almost a factor of four for ^{13}C–^{1}H. Heteronuclear spin systems couple (in a manner analogous to resonant circuits) producing a splitting of the resonance

peaks into multiplets whose type depends on spin multiplicity. This complicates the spectrum and reduces the peak height of already small resonances, making them harder to detect. The manifestation of J-coupling can be reduced or even eliminated by saturating the coupled spin partner during the acquisition with a second RF field $B_2 \gg 2\pi J/\gamma$, where J is the coupling between the two spin systems. The decoupling signal can be either continuous wave or, to increase the decoupling bandwidth, a series of composite pulses such as WALTZ or MLEV.[1]

When the proton channel is used only to acquire a scout image or shim the magnet, the RF coil can be switched between proton and non-proton mode, e.g., using PIN diodes, either to detune the inactive coil or to switch the resonance frequency of a single coil. NOE and polarization transfer, however, require simultaneous transmission on both the detected and decoupling channels; J-decoupling requires transmission on the decoupling channel while simultaneously acquiring the detected signal (Figure 5.2). These techniques place special requirements on the scanner hardware and the RF coil design. A scanner equipped for multinuclear studies is fitted with a complete second RF transmit and receive chain, often called the X-channel. Unlike the proton channel, which usually has a very narrow bandwidth, the X-channel is broadband, allowing it to be used for a range of different nuclei. The toughest demands on the RF system are from J-decoupling, where the decoupling transmit voltage is typically seven or more orders of magnitude larger than the detected NMR signal. Accurately recording this signal without interference from the decoupling is clearly an RF design challenge, requiring careful coil and system design.

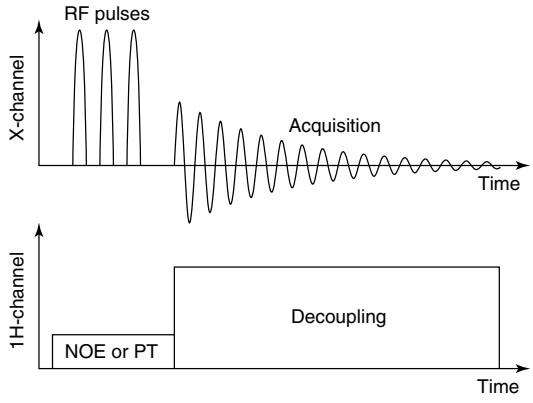

Figure 5.2. A typical multinuclear pulse sequence requires transmission on a second RF channel—for NOE or polarization transfer during transmission and J-decoupling during the acquisition.

5.3 BASIC SURFACE COILS

The simplest, and probably the most common, of all surface coils is a planar loop. The actual shape of a planar loop makes relatively little difference to the field it generates—circular and rectangular-shaped loops are both common. The magnetic field generated by a circular loop, oriented perpendicular to the y-axis, is shown as a map in the transverse plane in Figure 5.3(a). Surface coils are commonly curved to fit the surface of the sample, which helps to extend the magnetic field further into the sample. The circular loop in Figure 5.3(a) has been curved onto the surface of a z-oriented cylinder of twice the radius of the loop. All subsequent coil arrangements modeled in this chapter have been curved onto the same surface.

An alternative arrangement to a planar loop is a butterfly, or figure-of-eight, coil as shown in Figure 5.4(a). The generated field is concentrated closer to the coil than for a circular loop, and thus falls off more rapidly with increasing distance from the coil (Figure 5.3b). This can be useful if a very shallow field-of-view is required, for example, to avoid coupling to another nearby RF coil.

When designing a loop coil, the coil dimensions should be chosen to maximize the SNR of the signal detected from a given position, rather than the raw signal level. Consider a planar loop placed directly onto a semi-infinite conductive load, which is a good approximation when the load is much larger than the coil. The magnetic field on the loop axis, generated by the loop, is

$$B_1 = \frac{\mu_0 I}{2} \frac{R^2}{(y^2 + R^2)^{3/2}} \tag{5.1}$$

where R is the loop radius, and y is the distance into the sample. The signal voltage detected by the loop is

$$\xi = \omega_0 B_1 M_0 \Delta V \tag{5.2}$$

where M_0 is the sample magnetization, and ΔV is the voxel volume. The thermal noise voltage detected by

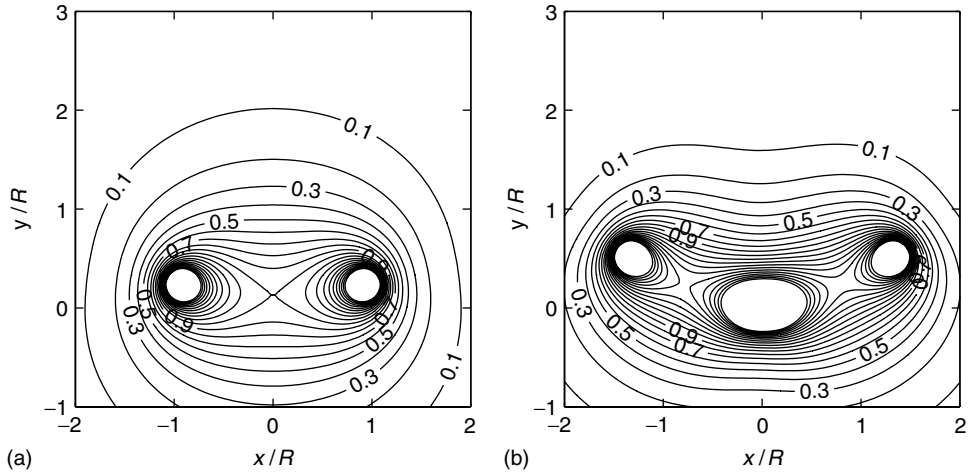

Figure 5.3. Transverse magnetic field B_{1xy} produced by (a) a circular loop and (b) a butterfly loop. Axes are normalized to the circular loop radius, and contour levels are relative to the field at the center of the circular loop. The butterfly loop was scaled to enclose the same area as the circular loop. The magnetic field in this and subsequent figures was numerically modeled using the Biot–Savart law.[4]

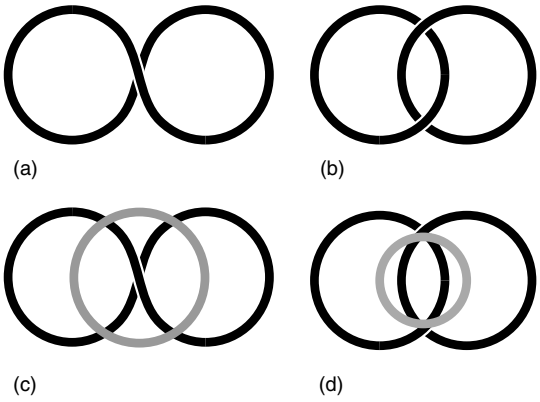

Figure 5.4. Coil designs: (a) a butterfly coil, (b) an optimally overlapped pair, (c) a quadrature butterfly, and (d) an Adriany–Gruetter coil.

the probe, which also depends on the field-of-view of the coil, is given by

$$N = \sqrt{4k_{\mathrm{B}}T_{\mathrm{s}}r_{\mathrm{s}}\Delta f} \tag{5.3}$$

where k_{B} is Boltzmann's constant, T_{s} is the sample temperature, and Δf is the bandwidth of the measurement. The effective resistance of the sample r_{s}, as seen by the loop, is

$$r_{\mathrm{s}} = \tfrac{1}{3}\mu_0^2\omega_0^2\sigma R^3 \tag{5.4}$$

where σ is the sample conductivity.[5] Finally, the SNR is given by

$$\psi = \frac{\xi}{N} \propto \sqrt{\frac{R}{\left(y^2 + R^2\right)^3}} \tag{5.5}$$

By differentiating equation (5.5) with respect to R, the depth of maximum SNR is found to be $R_0 = y/\sqrt{5}$. Equation (5.5) is the main design equation when planning a loop coil. A loop with a radius smaller than R_0 has insufficient sensitivity at the required depth, while a loop larger than R_0 is too sensitive to sample noise.

Plotting coil sensitivity and SNR (equations (5.1) and (5.5)) against loop radius clearly demonstrates that optimizing a loop coil to maximize B_1 intensity at a particular depth is not the same as optimizing the SNR at that depth (Figure 5.5). To stay within 90% of the optimum SNR, a loop coil should be designed such that $0.25 \leq R/y \leq 0.70$, where R is the coil radius and y is the depth of the target region.

The above analysis assumes that noise is generated only by the sample, and that the RF wavelength is large compared to the sample size. The proportion of noise generated by the sample, relative to that produced by the coil, may be determined by measuring the unloaded and loaded Q factors. For large coils, such as those used in human studies, sample noise in dominant (typically $Q_{\mathrm{U}}/Q_{\mathrm{L}} > 5$, indicating that more

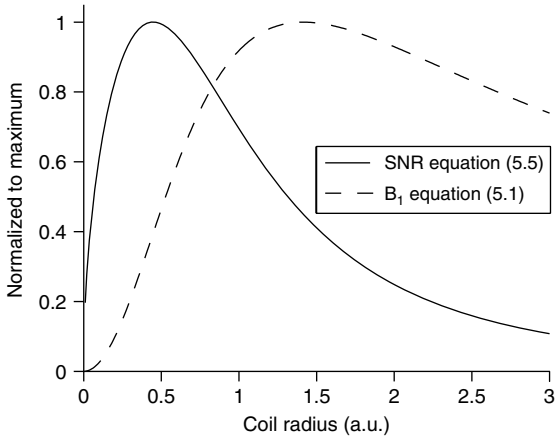

Figure 5.5. Variation in SNR and signal intensity, at unit depth, versus radius for a circular loop coil with a semi-infinite load.

than 80% of the total noise comes from the sample). With smaller coils, such as those used in small animal experiments, noise from the coil, due to losses in the conductor, capacitors and solder joints becomes more significant.[5] In this case, optimum SNR is achieved with a loop radius slightly larger than that predicted by equation (5.5).[6] At short wavelength, relative to the sample size, the sample has a significant influence on the B_1 field distribution, and full-wave electromagnetic simulations may be necessary to optimize the coil dimensions (see Chapter 27).

For lower frequency coils, it is sometimes necessary to add multiple turns to a coil, but it is important to realize that this does not improve the SNR. Consider, for example, adding a second turn to a circular loop to form a two-turn solenoid. The coil now "sees" twice as much signal from the sample. However, the noise level will also increase. There are two major sources of noise in an NMR experiment: thermal noise from the sample, and thermal noise from the coil. As the coil cannot distinguish between the NMR signal and thermal noise from the sample, increasing sensitivity to the signal also increases sensitivity to the noise by the same factor. At the same time, the coil now uses twice the length of wire as a single loop, doubling its resistance, and hence doubling its thermal noise contribution. The signal detected by the coil increases, but the noise increases by the same factor, and the SNR remains the same. Instead, the number of turns should be chosen to give a reasonable impedance at the resonance frequency, so that the loop can be resonated and matched to 50 Ω using achievable capacitor values.[7]

The opposite problem occurs at high frequency, as the RF wavelength approaches the conductor length of a single-turn loop. A significant phase shift is increasingly present along the length of the conductor, and the loop approaches transmission-line, rather than lumped-element, behavior. The current phase progression can be reduced by splitting the loop into two or more sections, separated by capacitors, such that each section is shorter than approximately a tenth of a wavelength. An added advantage of splitting the tuning capacitance in this manner is that it increases the required lumped capacitor values, which are otherwise often comparable to parasitic capacitances present around the loop, thus making the loop resonant frequency less sensitive to coil positioning with respect to the patient and other nearby conducting structures.

5.4 QUADRATURE

The NMR signal is generated by spins precessing about a magnetic field. This has an important consequence for the detected signal—it rotates in only one direction. When a single loop coil is used to detect the NMR signal, it operates in the linear mode. That is, it is sensitive to magnetic fields rotating in either direction about the static field. The main noise contribution comes in the form of thermal noise from the sample. Unlike the signal, the noise is not polarized, and is equally distributed between positive and negative rotating components. By making a coil insensitive to the counter-rotating field component, the noise power detected by the coil is halved without affecting the signal power. Because the measured NMR signal is a voltage, this increases the SNR by a factor of $\sqrt{2}$.[5,8]

Transmitting with a quadrature coil also offers significant benefit. Only the field component rotating in the same sense as spin precession produces a nutation. However, both the positive and negative rotating field components induce RF eddy currents in the sample, which cause Ohmic heating. An ideal quadrature coil generates no negative rotating field, and so halves the heating of the sample, while producing exactly the same spin nutation.

Production of a quadrature field requires two, ideally orthogonal, independently controllable magnetic fields. With surface coils, this is most commonly achieved by combining a pair of loop coils. When the

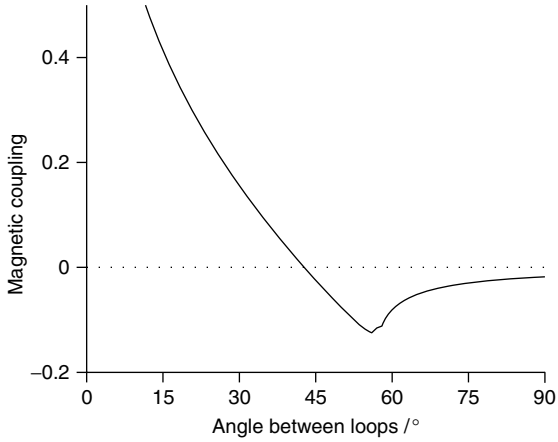

Figure 5.7. Inductive coupling between a pair of circular loops vs the angle between them. At approximately 43° overlap, the coupling is zero.

loops are positioned perpendicular to one another, the magnetic fields they generate are also approximately perpendicular, and the coupling between the loops is low. Figure 5.6 shows the positive and negative rotating fields generated by this arrangement. The pair generate a stronger positive than negative rotating field, but the efficiency is low, largely because the most sensitive region of one loop is in the periphery of the other.

To place the higher sensitivity regions closer together, the loops may be overlapped (Figure 5.4b). The loop fields are no longer perpendicular, causing the loops to inductively couple; the degree to which they couple depends on the size of the overlap. Outside the overlapped region, flux linkage between the loops creates a positive mutual inductance. Inside the overlapped region, the magnetic flux points in the opposite direction, and creates a negative mutual inductance. By carefully adjusting the overlap, the net mutual inductance can be minimized, at which point the loops are well decoupled.[9]

Figure 5.7 shows the mutual coupling between a pair of loops, wrapped onto a cylindrical surface, as a function of the angle between them. When the angle is small, i.e., close to a complete overlap, the coupling is very large. As the angle increases, the coupling reduces through zero to a negative minimum, and then increases back toward zero as the angle approaches 90°; in this particular case, the critical overlap is at approximately 43°. In practice, this overlap is best found by adjusting the loops at the bench, and monitoring the coupling between them with, e.g., a network analyzer. Figure 5.8 shows the positive and negative rotating fields generated by a pair of critically overlapped loops. In comparison to Figure 5.6, the intensity of the positive rotating field close to the loops is significantly increased, while the negative rotating field is decreased.

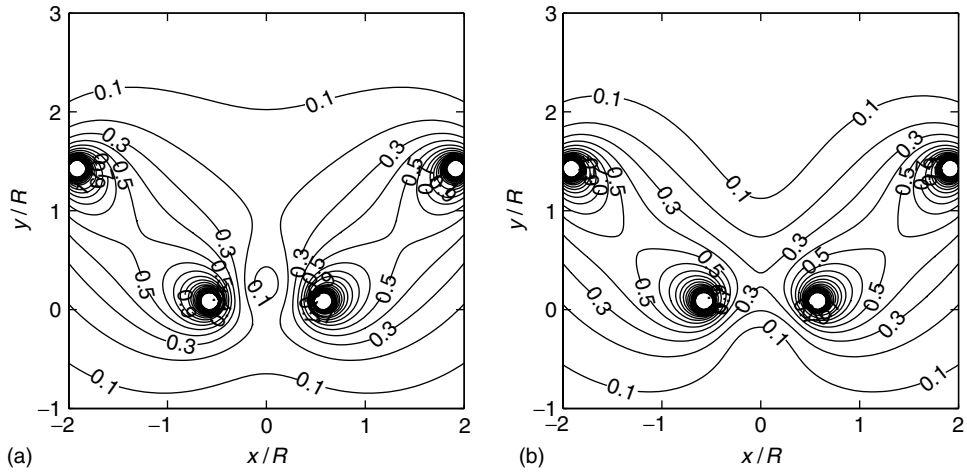

Figure 5.6. Transverse magnetic field B_{1xy} produced by a pair of perpendicular circular loops, rotating in the (a) positive and (b) negative direction. Field strength is relative to the field at the center of a single circular loop, and distances are given relative to the circular loop radius.

A quadrature pair can also be formed by combining a butterfly coil with a circular loop (Figure 5.4c). On one side of the pair, current flows in the same direction in the circular loop and the butterfly; on the opposite side, current in the butterfly opposes current flowing in the circular loop. Therefore, this arrangement is decoupled by symmetry, for any butterfly coil dimensions relative to the diameter of the circular loop.

It is clear from Figures 5.8 and 5.9 that surface coils do not produce a purely positive rotating B_1 field. The degree of polarization of the field may be characterized using

$$\beta = \frac{\left|\mathbf{B}_1^+\right|}{\left|\mathbf{B}_1^+\right| + \left|\mathbf{B}_1^-\right|} \tag{5.6}$$

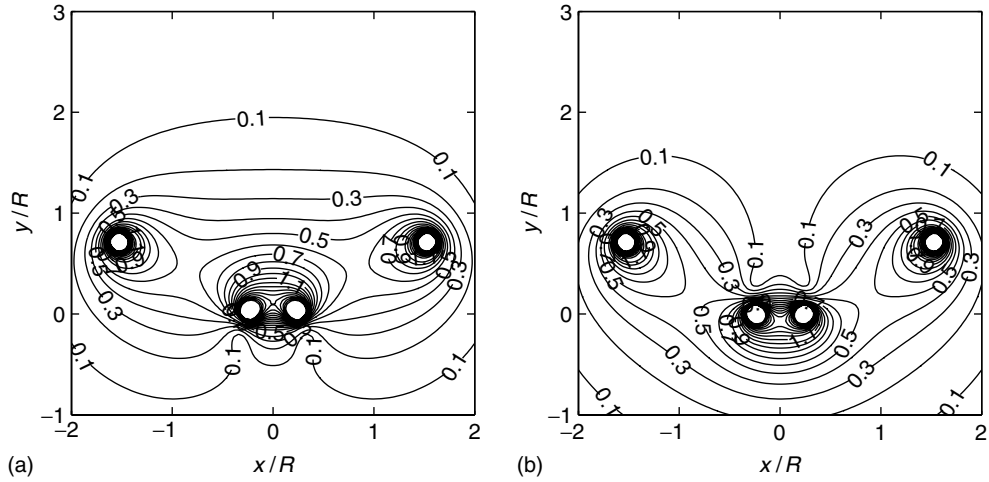

Figure 5.8. Transverse magnetic field B_{1xy} produced by a pair of optimally overlapped circular loops, rotating in the (a) positive and (b) negative direction. Field strength is relative to the field at the center of a single circular loop, and distances are given relative to the circular loop radius.

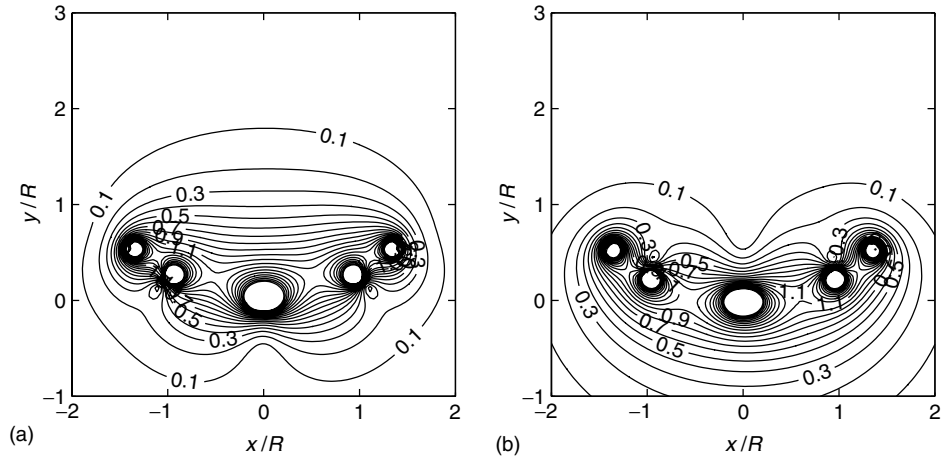

Figure 5.9. Transverse magnetic field B_{1xy} produced by a quadrature butterfly coil, rotating in the (a) positive and (b) negative direction. Field strength is relative to the field at the center of a single circular loop, and distances are given relative to the circular loop radius.

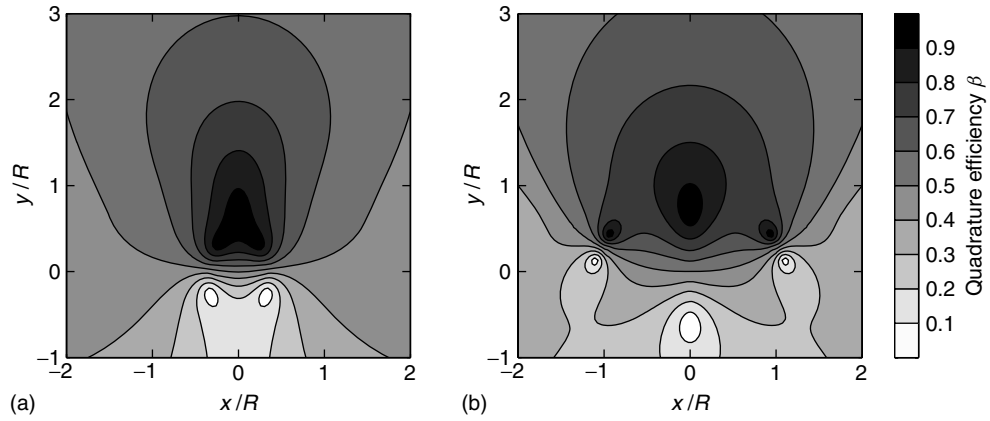

Figure 5.10. Maps showing the quadrature efficiency $\beta = \left|\mathbf{B}_1^+\right| / \left|\mathbf{B}_1^+\right| + \left|\mathbf{B}_1^-\right|$ of (a) an optimally overlapped pair, and (b) a quadrature butterfly coil.

where $\mathbf{B}_1^+$ and $\mathbf{B}_1^-$ are the positive and negative rotating field components.[10] A value of $\beta = 1$ indicates perfect quadrature, $\beta = 0$ is perfect antiquadrature (i.e., the field rotates in the wrong direction), and $\beta = 0.5$ indicates a linearly polarized field, with equal positive and negative rotating components. Over the region of optimum sensitivity, a surface coil should produce $0.5 \leq \beta \leq 1$. Figure 5.10 shows simulated β-maps for a pair of optimally overlapped loops, and for a quadrature butterfly coil. The butterfly pair produce a larger region of highly polarized field ($\beta > 0.7$) than the overlapped loops. However, Figure 5.10 has to be seen in combination with Figures 5.8 and 5.9. A highly polarized field offers little benefit if it is so weak that noise from other regions of the sample will dominate, as is increasingly the case with increasing distance from the butterfly pair.

Experimentally, the quality of a quadrature field may be assessed by reversing the connections to the RF coil, allowing us to detect the normally invisible counter-rotating field. An ideal quadrature coil will produce a bright image with the coil connected correctly, and no image with the connections reversed. In practice, there is usually some antiquadrature sensitivity toward the edge of the field-of-view, but there should be none at the center. The sensitivity profile of a coil can be assessed by acquiring images of a uniform phantom. This method works well for proton coils, but less well for coils tuned to a low-sensitivity nucleus where there is not enough signal to produce an image. One solution is to heavily dope the phantom, giving enough signal to produce an image. Alternatively, the coil can sometimes be retuned to another more sensitive nucleus with a similar gyromagnetic ratio. For example, a ^{13}C coil can often be retuned to ^{23}Na to perform this test, as $\gamma_{13C}/\gamma_{23Na} = 0.91$.

5.5 MULTINUCLEAR SURFACE COILS

The coils discussed so far are all designed to operate at a single frequency. This section introduces a selection of coils designed to operate at two frequencies, to enable the use of NOE and J-decoupling.

The key to a good multinuclear coil arrangement is high sensitivity on the X-channel, and good isolation between the different frequencies. There are essentially two ways to achieve this. The first is to tune a single coil to two frequencies.[11] A drawback of this type of design is the lack of freedom to individually optimize the RF fields at the two frequencies; the coil has the same field-of-view at both (this is no longer strictly true at high static field strength, as the wavelength at the ^{1}H frequency approaches the sample size; however, although the sensitivity profiles are different at the high and low frequencies, they still cannot be optimized separately). The second approach is to place two separate coils around the sample, tuned to different frequencies but having approximately the same field-of-view. This is the method examined in this chapter.

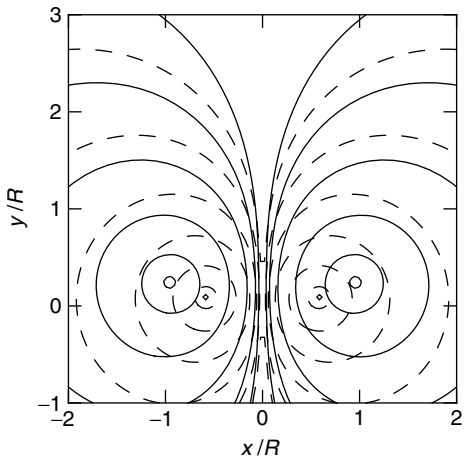

Figure 5.11. Flux line generated by a large loop (solid) placed concentrically around a smaller loop (dashed). The flux lines are almost parallel, producing high coupling between the loops.

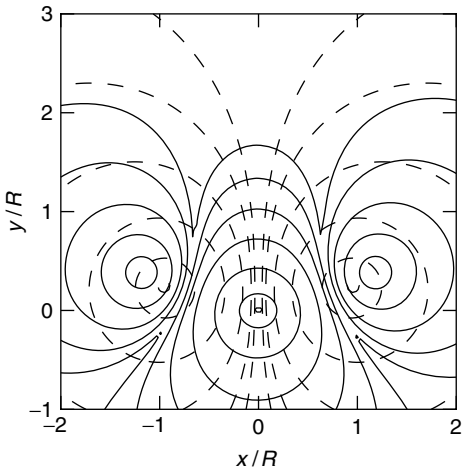

Figure 5.12. Magnetic flux lines between the butterfly (solid) and circular loop (dashed) are largely perpendicular.

A straightforward dual-coil design uses a large proton loop positioned concentrically around a smaller X-band loop, an arrangement which gives the proton coil a larger field-of-view than the X-coil.[12] This is often useful, as it is easier to plan the acquisition volume when more anatomy is visible, and the shimmed region should ideally be slightly larger than the acquired volume. It also ensures that the decoupling B_2 field completely covers the acquired volume. At the same time, the smaller size of the X-coil maximizes its sensitivity. The problem with this design becomes clear on examining the magnetic flux generated by the two loops (Figure 5.11); the flux lines are almost parallel, producing strong coupling between the coils. To decouple the coils, the flux lines generated by one coil should ideally be perpendicular to those generated by the other coil.

The butterfly coil, described in Section 5.4 (Figure 5.4c) as a single-frequency quadrature coil, can also be used as a dual-resonant linear coil.[13] Rather than using a symmetry argument, decoupling between a circular loop and a butterfly can be understood by considering the flux generated by the two loops (Figure 5.12). Flux generated by the butterfly is perpendicular to the flux generated by the circular loop, producing very low flux linkage between the pair, giving this coil design good separation between the two channels. Its disadvantages are a shallow sensitive volume, and that in terms of sensitivity and specific absorption rate (SAR), the benefit from operating the coil in quadrature mode is lost.

The Adriany–Gruetter design (Figure 5.4d) addresses this shortcoming by adding a third coil to the probe.[14] The design principle is similar to the double-resonant butterfly, but exchanges the butterfly loop for an optimally overlapped quadrature pair. Flux lines generated by the single loop, and each loop of the quadrature pair, are shown in Figure 5.13. In the center of the field-of-view, where the B1 intensity is strongest (Figures 5.3a and 5.8a), flux lines generated by each loop of the quadrature pair are largely perpendicular to those generated by the central loop (Figure 5.13), resulting in low coupling between quadrature pair and the single loop. The quadrature pair remain mutually decoupled as discussed in Section 5.4.

The overlapped pair are usually tuned to the proton frequency, with the smaller linear loop used for the X-band. This is important for human studies, as it halves the SAR deposited by the decoupler channel, which is the main SAR constraint in e.g. ^{13}C detection experiments. The loops of the quadrature pair are generally made slightly larger than the linear loop, to give a larger field-of-view at the proton frequency than the X-frequency, for the reasons described previously. The original design, built for human spectroscopy at 4 T, used 120 mm and 70 mm diameter loops, respectively. For small animal studies, where SAR is less of a concern, the overlapped pair

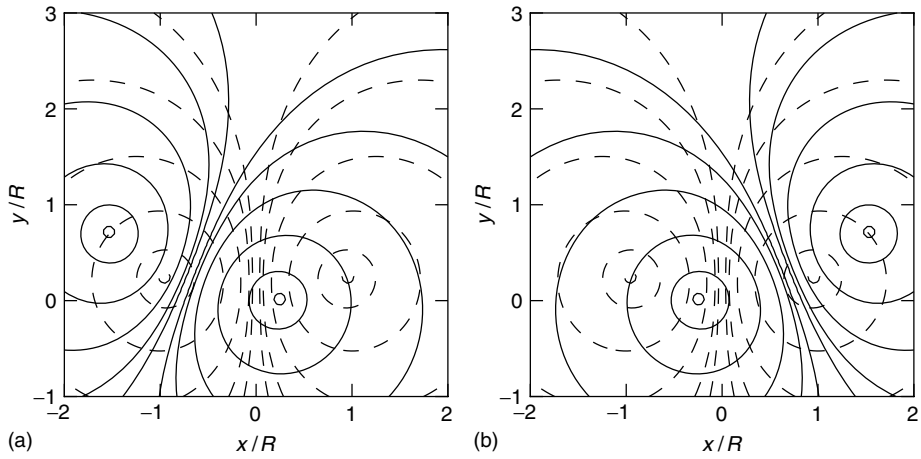

Figure 5.13. Magnetic flux lines generated by an Adriany–Gruetter coil. Flux lines generated by the (a) left and (b) right loops of the quadrature pair (solid) are almost perpendicular to the flux lines generated by the linear loop (dashed), resulting in low coupling between the ^{1}H and X coils.

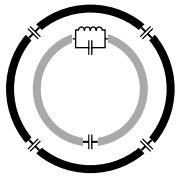

Figure 5.14. The lower frequency loop (inner) can be decoupled from the higher frequency loop (outer) by the addition of parallel-resonant trap circuit, tuned to the higher frequency. The loops are shown in a concentric arrangement, but as the decoupling does not depend upon geometry, any arrangement may be used.

can be tuned to the X-frequency, to attempt to take advantage of the $\sqrt{2}$ improvement in SNR, although the smaller field-of-view of the proton channel will give suboptimal J-decoupling.

Geometric decoupling of coils is very effective, but constrains the relative positions of the coils. An alternative approach to decoupling uses the fact that, in a multinuclear coil, different coil elements are tuned to different frequencies. Coupling is strongest at the higher frequency because, while the high frequency coil does not resonate below its fundamental frequency, the low-frequency coil can also resonate at higher harmonics. The problem is particularly acute for ^{13}C–^{1}H coils, as the proton frequency is almost exactly the forth harmonic of the ^{13}C coil.

Adding a parallel-resonant inductor–capacitor (LC) trap circuit to a coil splits the loop resonance into two peaks, an effect previously used to produce double-resonant coils.[11] More recently, the same circuit has been applied in a different manner, to prevent coupling at the higher frequency between a pair of loops tuned to two different frequencies (Figure 5.14).[15,16] The trap is tuned to the higher frequency, but inserted into the lower frequency loop. It blocks current flow at the higher frequency, preventing coupling between the two loops. At the low frequency, the trap presents a low inductive impedance, producing a slight shift in the loop resonance frequency, which can be corrected using the tuning capacitor. It is unfortunate that the trap must be added to the X-coil. While some sensitivity may be sacrificed on the ^{1}H channel, where the signal is stronger, the sensitivity of the X-channel is critical; care must be taken that the introduction of the trap circuit does not significantly reduce the performance at the X-frequency. However, with careful trap construction, SNR losses on the X-channel can be kept below 5%.[16]

Trap-decoupling provides an extra degree of freedom in multinuclear coil design, in that the arrangement of coil elements for the ^{1}H and X-channels can now be independently optimized. This opens up interesting possibilities such as an X-only surface coil combined with a ^{1}H volume coil,[17] or dual-frequency array coil design.

5.6 FILTERS

Although careful coil design can reduce interaction between the X- and ^{1}H-channels, further filtering is usually necessary to prevent significant noise injection from the decoupling channel into the observed channel.

RF power amplifiers are inherently noisy devices, typically having a noise figure above 10 dB, often generating noise over a far wider bandwidth than the amplifier's nominal operating range. In a homonuclear NMR experiment, the power amplifier output is usually gated off (disabled) during acquisition, to prevent noise from the amplifier entering the receiver. In a multinuclear experiment using J-decoupling, the decoupling power amplifier must be active during the acquisition. Placing a filter directly after the decoupling power amplifier, designed to block signal outside the transmit bandwidth, can reduce the noise level reaching the receive path. A bandpass filter is placed on the proton channel, while a low pass filter, which usually has a lower insertion loss, is preferred for the X-channel.

A second lower power filtering stage is often added between the receive coil and the preamplifier. Although the decoupling signal is generally outside the preamplifier bandwidth, a large out-of-band signal can saturate the preamplifier input, distorting the amplified signal. Placing a filter before the preamplifier can minimize this (Figure 5.15). The combination of coil decoupling and filtering should be strong enough to attenuate the decoupler signal down to the level of in-band thermal noise at the preamplifier input. Note that, as this filtering stage is placed before the preamplifier, its insertion loss is critical. A good filter can have an insertion loss as low as 0.1 dB, with 70 dB of attenuation in the stop-band.

5.7 SUMMARY

In vivo non-proton magnetic resonance is difficult because the signals are very small. However, the continued development of higher field systems makes non-proton magnetic resonance imaging and spectroscopy attractive. The RF design is further complicated by the need to transmit a proton signal, while receiving the nonproton signal. High sensitivity to the non-proton signal, and very strong decoupling between the proton and non-proton channels is key.

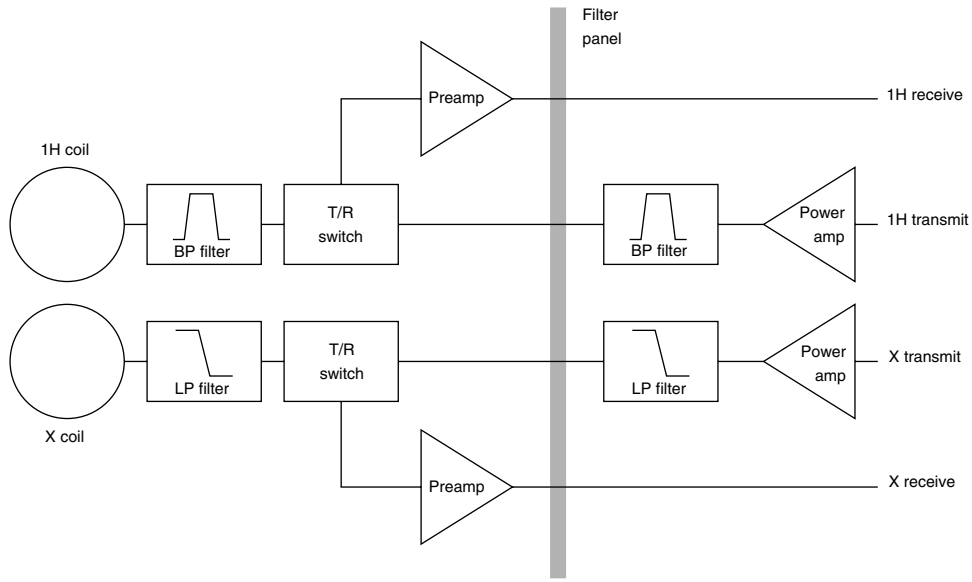

Figure 5.15. Filter placement for a multinuclear system. Filters directly after the power amplifiers prevent out-of-band noise from the amplifiers entering the RF chain. Filters between the coils and T/R-switches block the coupled signal, preventing saturation of the preamplifiers during J-decoupling.

Surface coils are ideal for non-proton magnetic resonance because they offer higher SNR than volume coils, albeit over a smaller field-of-view. Using separate coils for the different frequencies allows the field-of-view to be individually tailored at each frequency. However, careful design and construction is required to maintain the necessary decoupling between the different coils, using either a geometric or a trapped design. Finally, while good coil design is crucial to multinuclear magnetic resonance, system optimization is also important. In particular, filtering on both the observed and J-decoupling channels must be considered.

RELATED ARTICLES IN THE ENCYCLOPEDIA OF MAGNETIC RESONANCE

Brain MRS of Human Subjects

Decoupling Methods

Double Resonance in Liquids

Proton Decoupling During In Vivo Whole Body Phosphorus MRS

Radiofrequency Systems and Coils for MRI and MRS

Sensitivity of the NMR Experiment

Shimming of Superconducting Magnets

Sodium-23 Magnetic Resonance of Human Subjects

Surface and Other Local Coils for In Vivo Studies

Surface Coil NMR: Detection with Inhomogeneous Radiofrequency Field Antennas

REFERENCES

1. R. Freeman, *A Handbook of Nuclear Magnetic Resonance*, Longman Scientific & Technical: Harlow, 1988.
2. J. J. Ackerman, T. H. Grove, G. G. Wong, D. G. Gadian, and G. K. Radda, *Nature*, 1980, **283**, 167–170.
3. R. A. de Graaf, *NMR Spectroscopy: Principles and Techniques*, 2nd edn., John Wiley & Sons: Chichester, 2007.
4. J. Jin, *Electromagnetic Analysis and Design in Magnetic Resonance Imaging*, CRC Press: London, 1998.
5. C.-N. Chen and D. I. Hoult, *Biomedical Magnetic Resonance Technology*, IOP Publishing: Bristol, 1989.
6. A. Kumar, W. A. Edelstein, and P. A. Bottomley, *Magn. Reson. Med.*, 2009, **61**(5), 1201–1209.
7. J. Mispelter, M. Lupu, and A. Briguet, *NMR Probeheads: for Biophysical and Biomedical Experiments*, Imperial College Press: London, 2006.
8. D. I. Hoult, C.-N. Chen, and V. J. Sank, *Magn. Reson. Med.*, 1984, **1**(3), 339–353.
9. P. B. Roemer, W. A. Edelstein, C. E. Hayes, S. P. Souza, and O. M. Mueller, *Magn. Reson. Med.*, 1990, **16**, 192–225.
10. J. Wang, Q. X. Yang, X. Zhang, C. M. Collins, M. B. Smith, X. H. Zhu, G. Adriany, K. Ugurbil, and W. Chen, *Magn. Reson. Med.*, 2002, **48**(2), 362–369.
11. J. R. Fitzsimmons, H. R. Brooker, and B. Beck, *Magn. Reson. Med.*, 1989, **10**(3), 302–309.
12. J. Mispelter, B. Tiffon, E. Quiniou, and J. M. Loste, *J. Magn. Reson.*, 1989, **82**(3), 622–628.
13. P. A. Bottomley, C. J. Hardy, P. B. Roemer, and O. M. Mueller, *Magn. Reson. Med.*, 1989, **12**(3), 348–363.
14. G. Adriany and R. Gruetter, *J. Magn. Reson.*, 1997, **125**(1), 178–184.
15. M. Alecci, S. Romanzetti, J. Kaffanke, A. Celik, H. P. Wegener, and N. J. Shah, *J. Magn. Reson.*, 2006, **181**(2), 203–211.
16. A. Dabirzadeh and M. P. McDougall, *Concepts Magn. Reson.*, 2009, **35B**(3), 121–132.
17. D. W. Klomp, W. K. Renema, M. van der Graaf, B. E. de Galan, A. P. Kentgens, and A. Heerschap, *Magn. Reson. Med.*, 2006, **55**(2), 271–278.